Development of a sliding-tearing mode fracture mechanical tool for laminated composite materials

András Szekrényes

Abstract-This work presents the mixed-mode II/III pre-stressed split-cantilever beam specimen for the fracture testing of composite materials. In accordance with the concept of prestressed composite beams one of the two fracture modes is provided by the prestressed state of the specimen, and the other one is increased up to fracture initiation by using a testing machine. The novel beam-like specimen is able to provide any combination of the mode-II and mode-III energy release rates. A simple closed-form solution is developed using beam theory as a data reduction scheme and for the calculation of the energy release rates in the new configuration. The applicability and the limitations of the novel fracture mechanical test are demonstrated using unidirectional glass/polyester composite specimens. If only crack propagation onset is involved then the mixed-mode beam specimen can be used to obtain the fracture criterion of transparent composite materials in the G_{II} - G_{III} plane in a relatively simple way.

Keywords-Composite, Fracture mechanics, Toughness testing, Mixed-mode II/III fracture.

I. INTRODUCTION

The investigation of the interlaminar fracture toughness of composite materials is important due to their susceptibility to delamination caused by e.g. low-velocity impact, edge effect or combined mechanical load. Linear elastic fracture mechanics (LEFM) implies mode-I, mode-II and mode-III fracture conditions [1]. For mode-I and mode-II there are standard tools to help the design of composite structures with cracks and notches [2], [3]. The international standards (ASTM, ESIS) propose also fracture tools for the mixed-mode I/II cases [4], [5]. There is a quite different status considering the mode-III fracture of composites. Based on the state-of-art review of the present situation the following tools are available for mode-III delamination:

- the crack rail shear test (CRS) [6],
- the split-cantilever beam (SCB) [7],
- the edge-crack torsion (ECT) test [8]–[13],
- the modified version of the split-cantilever beam [14]–[18],
- the anticlastic plate bending (APCB) method [19],
- the mode-III four point-bend end-notched (4ENF$_{III}$) [20],
- the four-point bending plate test (4PBP) [21],
- the updated version of the modified split-cantilever beam [22],

A. Szekrényes is with the Department of Applied Mechanics, Budapest University of Technology and Economics, 1111 Budapest, Muegyetem rkp. 5., HUNGARY, phone: +36 1 463 1170, e-mail: szeki@mm.bme.hu

- the 6-point edge crack torsion (6ECT) [23],

where the systems can be classified into two essential groups: beam and plate specimens. This short review shows that the development of mode-III fracture tools is still in progress. The main reason for that is each system is useful and - more or less - works fine, in spite of that there are also significant drawbacks compared to the relatively simple mode-I and mode-II tests. Among others, the complex fixtures, the difficult data reduction and specimen preparation (mainly in plate specimens) can be mentioned. When a mode-III system is to be chosen, one of the aspects can be whether the system can be extended for mixed-mode I/III, II/III and I/II/III conditions or not. In this respect the composite literature offers the following mixed-mode configurations:

- the prestressed end-notched flexure (PENF$_{II/III}$) [24],
- the 8-point bending plate (8PBP, mixed-mode I/III) system [25],
- the 6-point bending plate (6PBP, mixed-mode II/III) system [26],
- the prestressed split-cantilever beam (PSCB$_{I/III}$) [27],
- the double-notched split cantilever beam (DNSCB, mixed-mode II/III) [28].

In the case of PENF$_{II/III}$ and PSCB$_{I/III}$ systems beam-like specimens are used, and one of the energy release rates is prestressed providing a fixed value, while the other component is increased up to fracture initiation. The advantages are that there is an analytical reduction technique, the specimen geometry is simple and both uni- and multidirectional lay-ups can be applied, however the drawbacks are that the mode ratio changes with the crack length and applied load [27]. The 6PBP and 8PBP systems apply cross-ply laminated plates subject to bending and because of that specimen preparation requires much effort [25], [26]. Moreover the data reduction is possible only by a finite element model including virtual crack-closure technique (VCCT) [29] and cohesive zone model (CZM) [25], [26] applications. The newest development is the DNSCB test, which eliminates the torsion in the SCB test by applying a double-notched beam with applied loads parallel to the delamination plane [28]. While in the case of the plate bending and prestressed beam specimens any mode ratios can be produced, in the DNSCB system it is not possible. This short introduction shows that this field of fracture mechanics is not sufficiently mapped, and that we need more elaborated tools to gain information on how the composite materials behave under the presence of the mode-III energy release rate.

This work is intended to develop a novel mixed-mode II/III fracture test. The original concept of prestressed composite

beams was applied first for mixed-mode I/II [30], later it was extended to II/III [24] and I/III [27] cases, respectively. Although the PENF$_{II/III}$ [24] worked, the crack length was restricted by the central load introductor of the three-point bending setup, on the other hand that was the mode-III energy release rate (ERR), which was initially prestressed. Due to the small compliance of the MSCB system the accuracy of the test was not satisfactory. In the present work we introduce the mixed-mode II/III version of the PSCB system. It will be shown subsequently that the previous analytical solutions can be used for data reduction of experiments performed on E-glass/polyester material. Then, a finite element analysis is conducted to show the distribution of the energy release rate during the fracture process. A fracture criterion based on the average energy release rate (over the specimen width) is introduced. Finally, the fracture envelope in the G_{II}-G_{III} is constructed and compared to those created in the G_I-G_{II} and G_I-G_{III} planes based on previous works.

II. THE PSCB SPECIMEN FOR MIXED-MODE II/III CRACKING

The PSCB$_{II/III}$ specimen is the combination of the end-loaded split (ELS) [31] and MSCB specimens [22]. Fig.1 shows the 3D model of the system developed in SOLID-WORKS. The main idea is based on the principle of superposition, i.e an ELS-MSCB combination, wherein the MSCB part is identical to that presented in previous papers [22], [32]. To produce mixed-mode II/III condition the specimen is put into a prestresser tool given by Fig.2. The exploded view shows that the notched shaft (No.5) is constrained by ball and roller bearings, therefore the specimen is free to rotation about the x axis and its end is fixed, as it is shown by the second figure. Eventually, by fixing the transverse (y) displacement the mode-II energy release rate can be set through an ELS configuration. The specimen together with the tool is put between the rigs of the MSCB system. In Fig.1b No.8 refers to the prestresser tool. In the sequel we treat the system as the superposition of the ELS and MSCB systems. The superposition scheme is shown in Fig.3.

III. ANALYSIS

As it is shown in Fig.3 the load denoted by P_{ELS} is related to the mode-II part of the ERR, while P_1 and P_2 are the loads related to the mode-III loading. Based on the equilibrium of the system we have: $P_1 = P_{MSCB} \cdot s_2/s_1$ and $P_2 = P_{MSCB} \cdot (1 + s_2/s_1)$, where P_{MSCB} is the load transferred through roller C, s_1 and s_2 are the distances between rollers A, B and C (see Fig.4). Fig.4 shows the 2D views of the prestressed specimen and the loading grips. The mode-II part of the ERR is fixed by the prestresser nut.

The MSCB loading rigs transfer a scissor-like load to the prestressed specimen through rollers A and B. The external load, P_{MSCB} is introduced through roller C using a testing machine. To ensure the position of rollers A and B along the thickness of the specimen, they were substituted by grub screws, which can be adjusted by using a screwdriver. The grub screws run over the prestresser tool, and at the end of the
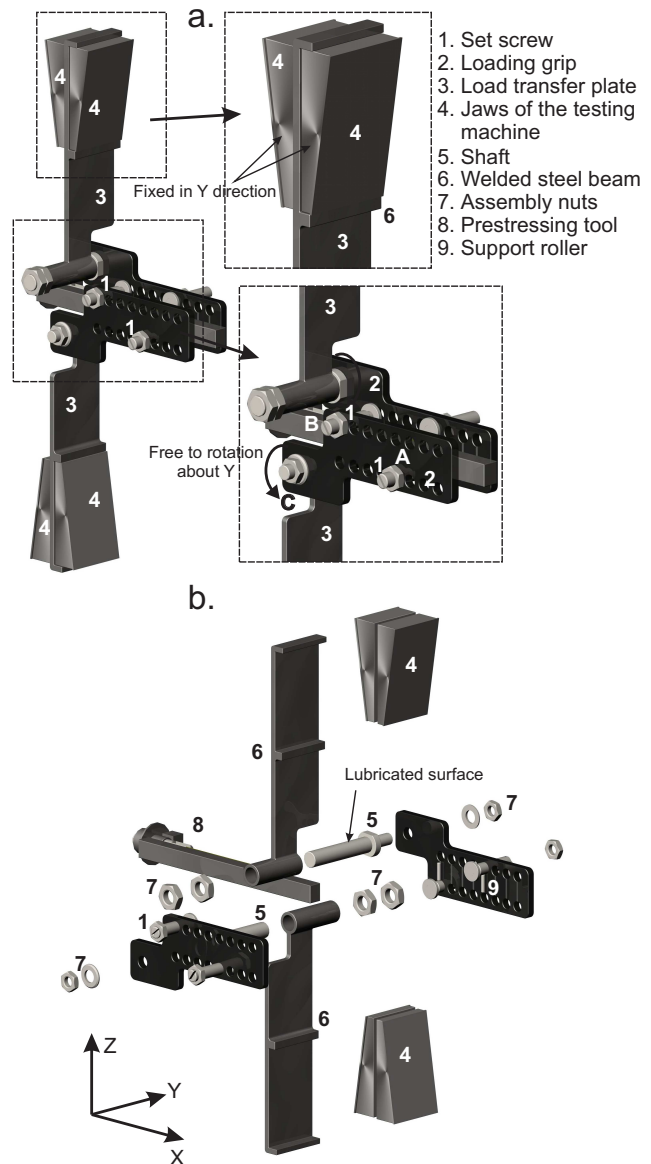

Fig. 1. The 3D views of the PSCB$_{II/III}$ specimen, assembled state (a), exploded view (b).

screws small disks were attached. By the proper adjustment of the axial position of the screws it is possible to realize that the disks belonging to the same grip have almost the same axial (y) position with respect to the x-z plane. This involves the rotation of the prestresser tool about the z axis, as shown by the top view in Fig.4. The moment equilibrium of the system about the x axis is ensured by the shaft and the tube part of the load transfer plate (refer to Fig.1). For the analysis of the PSCB$_{I/III}$ configuration we superimpose the solutions of the ELS and MSCB specimens. In some recent works [22], [32] the improved beam theory (IBT) solutions for the ELS and MSCB specimens were presented. The improved solution for the ELS specimen's compliance is [32]:

$$C_{ELS} = \frac{a^3}{2bh^3 E_{11}}[f_{EB1}^{ELS} + f_{TIM1}^{ELS} + f_{S-V}^{ELS} + f_{SH1}^{ELS}] \quad (1)$$

where:

$$f_{EB1}^{ELS} = 3 + \left(\frac{L}{a}\right)^3 \quad (2)$$

$$f_{TIM1}^{ELS} = \frac{1}{k}\frac{L}{a}\left(\frac{h}{a}\right)^2 \frac{E_{11}}{G_{12}} \quad (3)$$

$$f_{S-V}^{ELS} = \frac{6}{\pi}\left(\frac{L}{a}\right)^2 \left(\frac{E_{11}}{G_{12}}\right)^{\frac{1}{2}} \quad (4)$$

$$f_{SH1}^{ELS} = 0.98\left(\frac{h}{a}\right)\left(\frac{E_{11}}{G_{12}}\right)^{\frac{1}{2}} + 0.43\left(\frac{h}{a}\right)^2\left(\frac{E_{11}}{G_{12}}\right) \quad (5)$$

where a is the crack length, b is the specimen width, h is the half thickness, E_{11} is the flexural modulus of the specimen, furthermore, f_{EB1}^{ELS} is related to bending, f_{TIM1}^{ELS} captures transverse shear, f_{S-V}^{ELS} comes from the so-called Saint-Venant effect and f_{SH1}^{ELS} accounts for the crack tip shear deformation. Moreover, L is the span length in the ELS system, G_{12} is the shear modulus of the material in the x-y plane and $k=5/6$ is the shear correction factor.
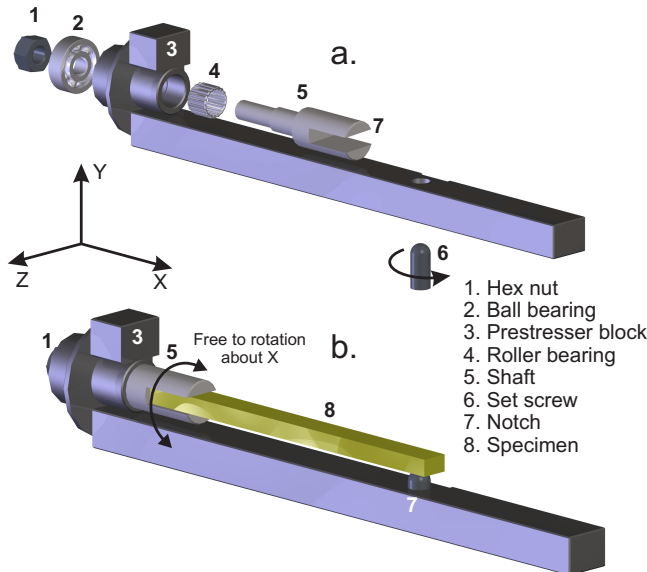

Fig. 2. Prestress tool for the $PSCB_{II/III}$ test, exploded view (a), assembled state (b).

The mode-II ERR of the ELS specimen can be obtained by using the Irwin-Kies expression [1]:

$$G_C = \frac{P^2}{2b}\frac{dC}{da} \quad (6)$$

which gives:

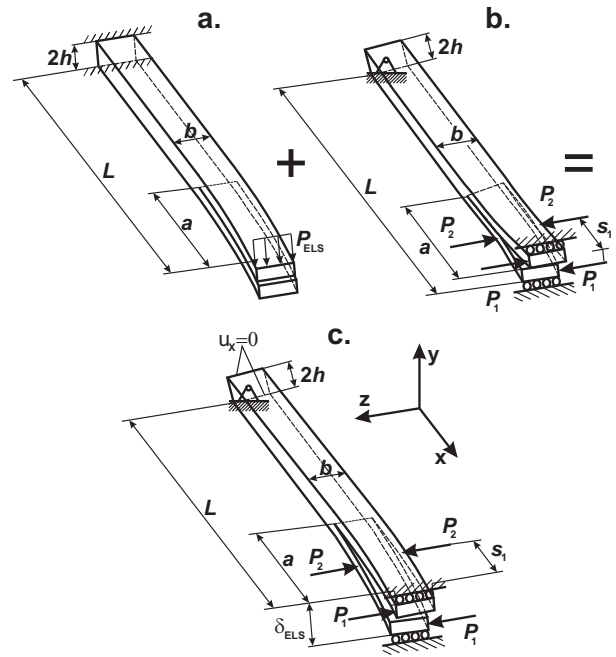$$G_{II}^{ELS} = \frac{P^2 a^2}{4b^2 h^3 E_{11}}[9 + f_{SH2}] \quad (7)$$

Fig. 3. The $PSCB_{II/III}$ specimen (c) as the superposition of the ELS (a) and MSCB (b) systems.
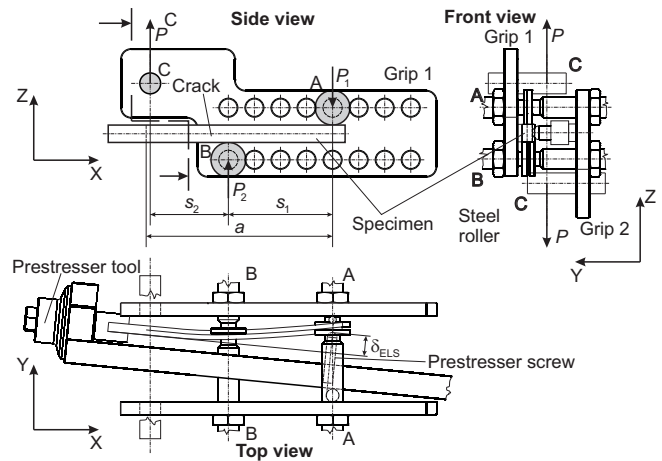

Fig. 4. The side, front and top views of the $PSCB_{II/III}$ system.

where f_{SH2} captures the crack tip shear deformation [32]:

$$f_{SH2} = 1.96\left(\frac{h}{a}\right)\left(\frac{E_{11}}{G_{13}}\right)^{\frac{1}{2}} + 0.43\left(\frac{h}{a}\right)^2\left(\frac{E_{11}}{G_{13}}\right) \quad (8)$$

As a next step we express the force in the ELS system subjected to imposed end displacement, which is possible to obtain from Eq.(1) using the definition of $C_{ELS} = \delta_{ELS}/P_{ELS}$:

$$P_{ELS} = \frac{\delta_{ELS}2bh^3 E_{11}}{a^3}\frac{1}{f_{EB1}^{ELS} + f_{TIM1}^{ELS} + f_{S-V1}^{ELS} + f_{SH1}^{ELS}} \quad (9)$$

Substituting Eq.(9) into Eq.(7) we have:

$$G_{II}^{ELS} = \frac{\delta_{ELS}^2 h^3 E_{11}}{a^4} \frac{9 + f_{SH2}}{(f_{EB1}^{ELS} + f_{TIM1}^{ELS} + f_{S-V1}^{ELS} + f_{SH1}^{ELS})^2} \tag{10}$$

The analysis of the MSCB specimen is detailed in [22]. The improved model takes four mechanical deformations into account: bending and shearing of the specimen arms, the Saint-Venant effect at the crack front and the free torsion effect in the delaminated portion. The compliance and the ERR calculated by the analytical solution were compared to the results of a three-dimensional finite element model and an excellent agreement was found. Since the MSCB specimen is loaded at four points it should be mentioned that the compliance is calculated at the point of external load application, i.e. at roller C in Fig.4, apparently, the compliance can be measured only at this point. The compliance of the MSCB specimen is:

$$C_{MSCB} = \frac{8a^3}{b^3 h E_{11}}[f_{EB1}^{MSCB} + f_{TIM1}^{MSCB} + f_{FT1}^{MSCB} + f_{S-V1}^{MSCB}], \tag{11}$$

where the terms in the brackets consider bending, transverse shear, free torsion and Saint-Venant effect in the MSCB specimen:

$$\begin{aligned} f_{EB1}^{MSCB} =& 1 - 3\left(\frac{s_1 + s_2}{a}\right) + 3\left(\frac{s_1 + s_2}{a}\right)^2 \\ & - \frac{s_1(s_1 + s_2)(s_1 + 2s_2)}{a^3} \end{aligned} \tag{12}$$

$$f_{TIM1}^{MSCB} = 0.3(1 - \frac{s_2^2 - s_1^2}{as_1})\left(\frac{b}{a}\right)^2 \left(\frac{E_{11}}{G_{13}}\right) \tag{13}$$

$$f_{FT1}^{MSCB} = 0.19\frac{1}{\varsigma}(1 - \frac{s_1}{a})\left(\frac{b}{a}\right)^2 \left(\frac{E_{11}}{G_{12}}\right) \tag{14}$$

$$f_{S-V1}^{MSCB} = 0.48\left(\frac{a - (s_1 + s_2)}{a}\right)^2 \left(\frac{b}{a}\right) \left(\frac{E_{11}}{G_{13}}\right)^{\frac{1}{2}} \tag{15}$$

and:

$$\varsigma = 1 - 0.63\mu\frac{h}{b}, \mu = \left(\frac{G_{13}}{G_{12}}\right)^{\frac{1}{2}} \tag{16}$$

where G_{13} is the shear modulus in the x-z plane, s_1 and s_2 are the distances between the loading rollers A, B and C, respectively (see Fig.4). Based on Eq.(6) the ERR is given by:

$$\begin{aligned} G_{III}^{MSCB} =& \frac{12P_{MSCB}^2 a^2}{b^4 h E_{11}} \cdot \\ & \cdot [f_{EB2}^{MSCB} + f_{TIM2}^{MSCB} + f_{FT2}^{MSCB} + f_{S-V2}^{MSCB}] \end{aligned} \tag{17}$$

where P_{MSCB} is the applied load of the MSCB specimen, furthermore:

$$f_{EB2}^{MSCB} = 1 - 2\left(\frac{s_1 + s_2}{a}\right) + \left(\frac{s_1 + s_2}{a}\right)^2 \tag{18}$$

$$f_{TIM2}^{MSCB} = 0.1\left(\frac{b}{a}\right)^2 \left(\frac{E_{11}}{G_{13}}\right) \tag{19}$$

$$f_{FT2}^{MSCB} = 0.06\frac{1}{\varsigma}\left(\frac{b}{a}\right)^2 \left(\frac{E_{11}}{G_{12}}\right) \tag{20}$$

$$f_{S-V2}^{MSCB} = 0.32\left(1 - \frac{s_1 + s_2}{a}\right)]\left(\frac{b}{a}\right)\left(\frac{E_{11}}{G_{13}}\right)^{\frac{1}{2}} \tag{21}$$

The condition of at least a 96% mode-III dominant test is [22]:

$$1.02 \le a/(s_1 + s_2) \le 1.09 \tag{22}$$

Combining Eq.(9) with (16) the mode ratio of the PSCB$_{II/III}$ specimen becomes:

$$\frac{G_{II}}{G_{III}} = \frac{b^4 h^4 E_{11}^2}{12a^6}\left(\frac{\delta_{ELS}}{P_{MSCB}}\right)^2 f_{II/III} \tag{23}$$

where:

$$\begin{aligned} f_{II/III} =& (9 + f_{SH2}) \cdot \\ & \frac{(f_{EB2}^{MSCB} + f_{TIM2}^{MSCB} + f_{FT2}^{MSCB} + f_{S-V2}^{MSCB})}{(f_{EB1}^{ELS} + f_{TIM1}^{ELS} + f_{S-V1}^{ELS} + f_{SH1}^{ELS})^2} \end{aligned} \tag{24}$$

All of the factors in Eq.(24) have been given before. The accuracy of the analytical solution has already been proved in previous papers [22], [24], [27]. It will be shown later that Eq.(23) represents the ratio of the average energy release rates along the crack front.
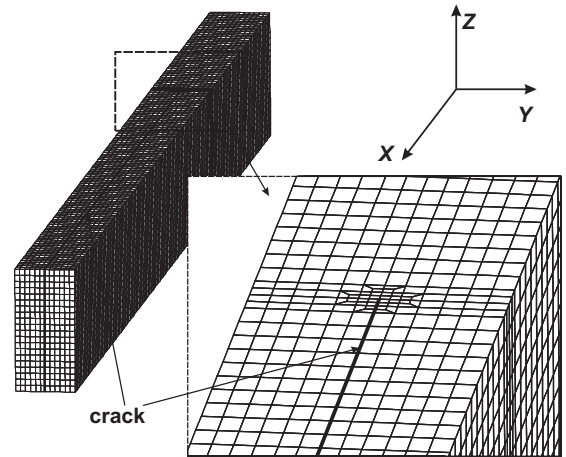

Fig. 5. The ANSYS finite element model of the PSCB$_{II/III}$ system.

IV. FINITE ELEMENT MODEL, VCCT

A finite element model shown in Fig.5 was created in the code ANSYS 12. The elastic properties of the models were: E_{11}=33 GPa, E_{22}=E_{33}=7.2 GPa, G_{12}=G_{13}=G_{23}=3 GPa and $\nu12$=$\nu13$=$\nu23$=0.27. The geometric properties were: b=12.8 mm, $2h$=6.2 mm, s_1=57.38 mm, s_2=49.36 mm and the length of the models was L=118 mm (refer to Fig.1). The three-dimensional model of the MSCB specimen was built using

linear eight-node SOLID brick elements. The imposed boundary conditions and the loading of the model are demonstrated in Fig.6. First, the model was loaded at the end of the specimen arm by a displacement value equal to δ_{ELS}=4.6875, 6.25, 8.125, 9.375, 10.625, 11.875 and 13.75 mm providing the mode-II part of the mixed-mode II/III ERR. These values were calculated from the number of revolutions and the pitch (1.25 mm) of the prestressing screw. On the other hand the model was also loaded in planes parallel to the delamination (from $h/2$ distance to the specimen side) applying the load values (P_1 and P_2) which were calculated using the experimentally measured P_{MSCB} loads based on crack initiation tests ($P_1 = P_{MSCB} \cdot s_2/s_1$ and $P_2 = P_{MSCB} \cdot (1 + s_2/s_1)$).
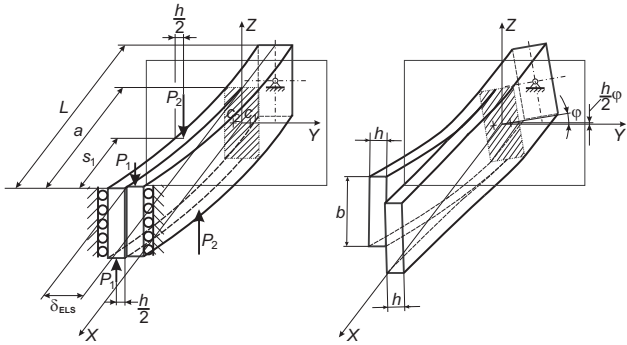

Fig. 6. The applied kinematic and dynamic boundary conditions in the finite element model and the deformation of the PSCB$_{II/III}$ specimen.

In the crack tip a refined mesh was constructed and the mode-II and mode-III ERRs were evaluated by using the virtual crack-closure technique (VCCT) [29], the size of the crack tip elements were $\Delta x=\Delta y$=0.25 mm and Δz=0.64 mm (refer to Fig.5 for the coordinate system). Fig.7 shows the distribution of the ERRs along the crack front in the case of δ_{ELS}=6.25, 10.625 and 13.75 mm. Based on the figures we can see that the mode ratio G_{II}/G_{III} changes significantly over the specimen width. As it can be seen both the mode-II and mode-III ERRs have an asymmetric distribution along the crack front. Therefore an assumption is necessary when we use this test to develop the fracture envelope of the material. In Fig.7 the average ERRs were obtained by dividing the integrated area under the curves by the specimen width. Table I. shows the comparison of the IBT to the VCCT results with respect to the average ERR and average mode ratio. The IBT underestimates G_{II} at most with 24.3% and underestimates G_{III} at most with 24.6%. This results in a maximum difference of -32.83% in the mode ratio. The disagreement at these points can be explained by the violation of Eq.(22), because in our case $s_1 + s_2$=57.38+49.36=106.74 mm. The error can be attributed to the wrongly designated geometrical parameters and not to the analytical model. It must also be noted, that the position of the loading screws was fixed, and due to the given specimen width we were not able to choose better positions for s_1 and s_2.

Although at some points there is not a so good agreement in Table I, it will be shown later that the fracture envelope obtained by the VCCT is almost the same as that of the IBT.
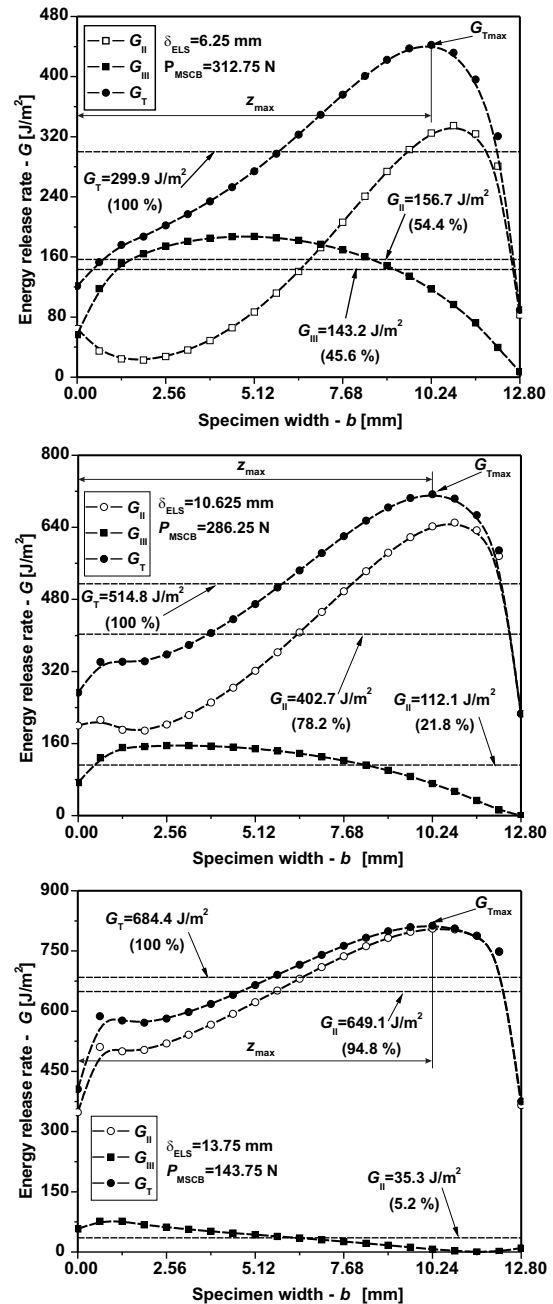

Fig. 7. The distribution of the mode-II, mode-III and total energy release rates along the specimen width.

Based on these results the IBT scheme is a possible data reduction scheme for the PSCB$_{II/III}$ test. Since the ERR varies along the crack front the specimen possess a curved crack front under crack propagation. Accordingly, as it is seen in Fig.7 a constant mode ratio along the crack front is not possible to be produced. Consequently, some assumptions are required considering the reduction of the experimental data.

V. AVERAGE ENERGY RELEASE RATE CRITERION

In the data reduction and calculation of G and G_{II}/G_{III} the widthwise average values will be adopted. During the

fracture process it is assumed that there exists a critical ERR, which is a material property. Moreover, the crack initiates if the widthwise average of the total energy release rate exceeds the critical value. The crack initation is expected at the point, where - in accordance with the distributions in Fig.7 - the local maximum of the distribution, G_{Tmax} appears. Although the possible errors in the analytically obtained mode ratio is relatively high, we prefer the IBT as a data reduction scheme, because the finite element analysis requires much computational time. Moreover, the same assumption would be required if we applied the VCCT to reduce the experimental data. It has already been shown that the IBT agrees excellently with the widthwise average G if we choose the parameters to satisfy Eq.(22) [24], [27]. It should be mentioned that a similar variation of the mode ratio exists in the other systems too [25], [26], [28]. An advantage of the $PSCB_{II/III}$ over the other tests is that the complete $G_{II} - G_{III}$ plane can be covered and an analytical reduction technique exists. In the sequel the details of the experimental work is presented.

VI. EXPERIMENTS

A. Material properties

The details of the specimen preparation and the determination of the material properties of the E-glass/polyester composite material was presented in several other papers [22], [24], and therefore we give only the followings: E_{11} =33 GPa, $E_{22} = E_{33}$ =7.2 GPa, $G_{12} = G_{13}$ =3 GPa and $\nu_{12} = \nu_{13}$ =0.27.

B. End-loaded split test

In the case of the ELS test (Fig.1b) we refer to previous fracture experiments [33] performed for a=105 mm. Four specimens were tested and it has been found that the initation ERR was G_{IIC}=706.8$\pm$ 32.6 J/m^2 evaluated by using an IBT scheme. This value will be used in the sequel.

C. Modified split-cantilever beam test

For the MSCB measurements four specimens were prepared with a=105 mm and s_1=57.38 mm, s_2=49.36 mm, respectively. Each specimen was put into the loading rig shown in Fig.1 (or detailed in [22]), the rig was adjusted in order to eliminate any play of the specimens. Then the specimens were tested, the load and displacement values were read from the scale of the testing machine and using a digitronic indicator. The crack initiation was identified by naked eye and when the first non-uniformity in the previously straight crack front was observed it was believed to be the point of crack initiation.

To justify the average energy release rate criterion an additional measurement was done by the MSCB specimen with s_1=25.69 mm, s_2=22.01 mm, respectively and using four specimens again. The crack length was also a=105 mm. Based on the finite element analysis of the system with these geometrical parameters it has been found that the average mode ratio is G_{II}/G_{III}=0.64. This condition is almost equivalent to that of the original split-cantilever beam test. It has been shown that in this case the distribution of the mode-II and mode-III ERRs is symmetric over the specimen width [34], [35].

D. Prestressed split-cantilever beam test

The experimental equipment for the $PSCB_{II/III}$ test is demonstrated in Fig.8. The tests were carried out using an Amsler testing machine under displacement control. The crack length of interest was a=105 mm. The critical specimen end displacement measured from the ELS test [33] is about 14 mm (if a=105 mm and L=118 mm). According to this fact, seven different values of the ELS displacement δ_{ELS} were set: 4.6875, 6.25, 8.125, 9.375, 10.625, 11.875 and 13.75 mm. The setup and the concept of the system is shown in Fig.1. Similarly to the MSCB tests, we applied four coupons at each displacement value. The load-deflection data was measured by using the scale of the testing machine and a digitronic indicator (see Fig.8). In each case the critical load at crack initiation was determined.
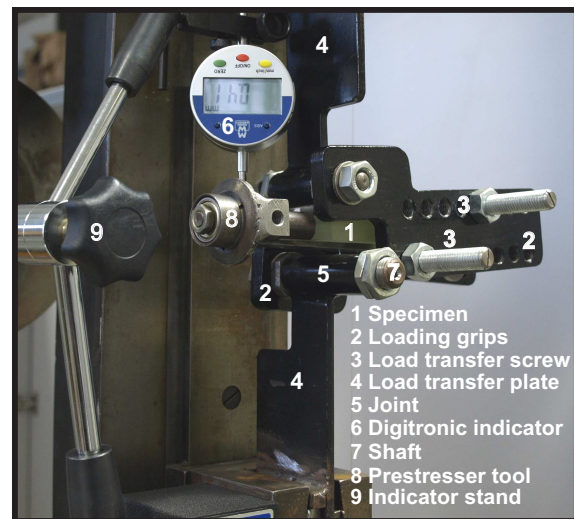

1 Specimen
2 Loading grips
3 Load transfer screw
4 Load transfer plate
5 Joint
6 Digitronic indicator
7 Shaft
8 Prestresser tool
9 Indicator stand

Fig. 8. The experimental equipment of the $PSCB_{II/III}$ system.

VII. RESULTS AND DISCUSSION

It will be shown subsequently that the stiffness, the compliance and the mode-III ERR of the $PSCB_{II/III}$ specimen are identical (with a very good approximation) to those of the MSCB specimen.

A. Load and displacement

Fig.9a shows a recorded load-displacement trace for the $PSCB_{II/III}$ specimen if δ_{ELS}=11.875 mm. The response follows essentially a linear relation. The $PSCB_{II/III}$ test was performed according to the followings. The onset of crack advance was identified by visual observations. In each case four specimens were tested, one of them was used to investigate the crack front. The other three specimens were loaded continuously and the crack initiation was observed in situ. Accordingly, the former specimen was loaded subsequently, at some points, where the initiation was expected the specimen was relieved, removed from the rig and the crack front was photographed. When the first non-uniformity was observed, then this point was denoted to be the point of

fracture initiation. The results of this process are demonstrated in Fig.9b for the $PSCB_{II/III}$ system at a prestressed state with δ_{ELS}=11.875 mm.
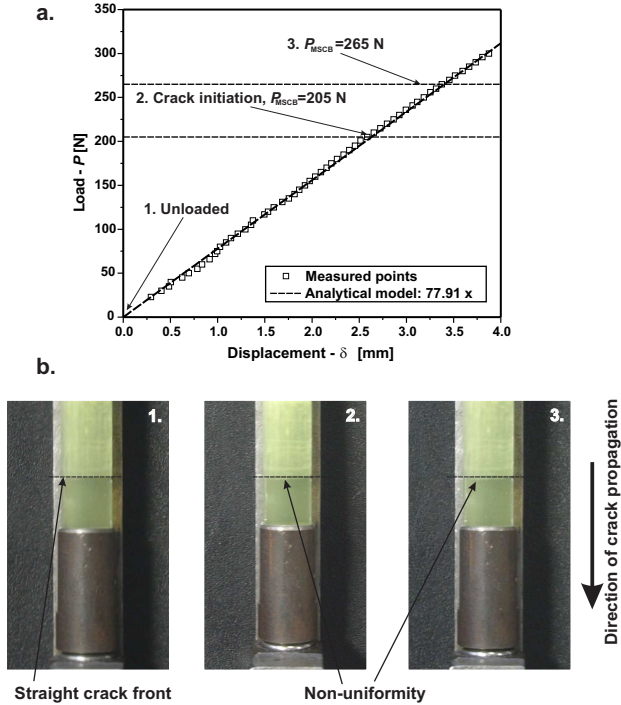

b.

Fig. 9.   The load-displacement curve of the $PSCB_{II/III}$ system for δ_{ELS}=11.375 mm (a). The identification of crack initiation during the fracture process (b).

B. Data reduction

Two reduction techniques (IBT and direct beam theory (DBT)) were applied to reduce the experimental data. In some recent works [27], [33] for the mixed-mode I/III version of the PSCB specimen and the mixed-mode I/II PELS system three reduction schemes were utilized: IBT, DBT and the finite element method. It has been shown that the optimal solution is the application of IBT, which was justified by the relatively small compliance of the MSCB specimen and the complexity of the finite element data reduction.

1) Improved beam theory: ELS specimen: In Eq.(7) P_{ELS} should be replaced with P_{II} (the load value at crack initiation in the ELS specimen) in order to obtain the improved analytical expression for the ERR of the ELS specimen (G_{IIC}=706.8$\pm$ 32.6 J/m^2 from IBT [33]).

MSCB specimen: Replacing P_{MSCB} with P_{III} in Eq.(17) gives the improved solution for the MSCB coupon, where P_{III} is the critical load value at crack onset. The IBT resulted in G_{IIIC}=114.5$\pm$16.0 J/m^2.

Prestressed split-cantilever beam specimen: The improved analytical solutions are given by Eqs.(10) and (17) for the $PSCB_{II/III}$ system.

2) Direct beam theory: ELS specimen: In the case of the $PSCB_{II/III}$ the displacement, δ_{ELS} is given by the prestresser tool's nut, while the force of the ELS part can be calculated

only by a model (analytical or finite element). Therefore, the application of DBT has no sense in our case and we replace the DBT result with that of IBT.

MSCB specimen: In accordance with DBT it is possible to obtain the following scheme for the MSCB specimen:

$$G_{DBT}^{MSCB} = \frac{3P_{III}\delta_{MSCB}}{2ba} \cdot$$
$$\left(\frac{f_{EB2}^{MSCB} + f_{TIM2}^{MSCB} + f_{FT2}^{MSCB} + f_{S-V2}^{MSCB}}{f_{EB1}^{MSCB} + f_{TIM1}^{MSCB} + f_{FT1}^{MSCB} + f_{S-V1}^{MSCB}} \right) \tag{25}$$

where the coefficients in the parentheses are given by Eqs.(12)-(16) and (18)-(21). In Eq.(25) P_{III} and δ_{MSCB} are the experimentally measured load and displacement values at the point of crack initiation in the MSCB specimen.

Prestressed split-cantilever beam specimen: We obtain the DBT scheme for G_{III} of the $PSCB_{II/III}$ system if we replace P_{II} with P_{ELS} in Eq.(5) and P_{III} with P_{MSCB} in Eq.(25). The application of DBT requires also the knowledge of additional material properties (E_{22}, G_{12}, G_{13}) of the applied composite material.

C. Critical energy release rates

The critical mode-II, mode-III and the mixed-mode II/III ERRs at crack initiation and the mode mix calculated by the IBT are given in Table I. The geometries tested had properties of a =105 mm, $2h$=6.2 mm, s_1=57.38 mm, s_2=49.36 mm, L=150 mm for the ELS test and L=118 mm for the $PSCB_{II/III}$ and at each value of δ_{ELS} four coupons were used. Table II presents the results obtained by the DBT scheme. The critical displacements (at crack initiation) were determined by the slopes of the load displacement curves. Using the critical displacements and the measured critical forces (P_{MSCB}) Eq.(25) was evaluated. In fact the scatter of the mode-II ERR component is zero, this is because the mode-II ERR is provided by the preload of the specimen. Comparing Tables I and II the difference between the G_{III} values - as well as the mode ratio - by DBT and IBT is not significant, the biggest difference was experienced at δ_{ELS}=6.25 mm. Overall the agreement is very good.

It is important to recommend a data reduction technique for the $PSCB_{II/III}$ system. The reliability and simplicity of the IBT has already been proved (e.g.: [22], [36], [37]). On the other hand the application of the FEM as a data reduction method requires large computational time, while IBT is more conservative than DBT. Accordingly, it is straightforward that at the present stage the optimal solution is the application of IBT for the evaluation of both the mode-II and mode-III ERRs, however it must be kept in mind that the data was evaluated assuming the average energy release rate criterion. Obviously, giving lower G_{III} values than the VCCT, the IBT is more conservative than the VCCT. Finally, the role of additional material properties (E_{22}, E_{33}, G_{12}, G_{13}, ν_{12}, ν_{13}) should be discussed. All of these parameters is determined by simple rule of mixture, therefore their accuracy is questionable. In some recent works similar prestressed systems to the present

TABLE I
COMPARISON OF THE ERRS AND MODE RATIOS BY BEAM AND FINITE ELEMENT ANALYSIS.

ELS displacement	δ_{ELS} [mm]	0(MSCB)	4.6875	6.25	8.125	9.375	10.625	11.875	13.75	14(ELS)
Load at crack initiation	$P_{MSCB}[N]$	247.8[1]	338.75	329.0	311.5	297.5	286.25	211.75	143.75	0
G_{II} [J/m^2]	IBT[a]	-	75.6	134.3	227.0	302.3	388.3	485.0	650.2	706.8
	VCCT widthwise av.[b]	-	99.9	156.7	246.2	318.9	402.7	490.5	649.1	724
	Difference $(a-b)/b$ [%]	-	-24.3	-13.0	-7.8	-5.2	-3.6	-1.1	0.2	-2.5
G_{III} [J/m^2]	IBT[a]	114.8	146.8	138.4	124.1	113.3	104.8	57.5	26.5	-
	VCCT widthwise av.[b]	121.9	151.0	143.2	129.7	119.5	112.1	64.8	35.3	-
	Difference $(a-b)/b$ [%]	-6.1	-2.8	-3.3	-4.3	-5.2	-6.5	-11.3	-24.6	-
G_{II}/G_{III}	IBT[a]	∞	0.51	0.97	1.82	2.67	3.70	8.44	24.42	-
	VCCT widthwise av.[b]	∞	0.66	1.09	1.90	2.67	3.59	7.57	18.39	-
	Difference $(a-b)/b$ [%]	-	22.2	11.34	3.62	-0.032	-3.06	-11.51	-32.83	-

[1]$s_1 = 49.25$ mm, $s_2 = 51.15$ mm

TABLE II
CRITICAL ENERGY RELEASE RATES CALCULATED BY THE DBT METHOD.

ELS displacement	δ_{ELS} [mm]	0(MSCB)[2]	4.6875	6.25	8.125	9.375	10.625	11.875	13.75	14(ELS)
Direct beam theory (DBT)	G_{II}/G_{III}	0	0.51	0.91	1.76	2.62	3.71	8.49	24.43	∞
		-	±0.03	±0.10	±0.18	±0.21	±0.32	±0.73	±6.06	-
	G_{II} [J/m^2]	0.0	75.6	134.3	227.0	302.3	388.3	485.0	650.2	706.8 (IBT)
	G_{III} [J/m^2]	100.5	149.4	149.6	130.1	115.9	105.3	57.4	28.1	0.0
		±16.3	±8.3	±17.2	±14.3	±9.2	±9.1	±5.0	±8.2	-
	G_T [J/m^2]	100.5	225.0	283.9	357.1	418.1	493.6	542.4	678.4	706.8 (IBT)

[2]$s_1 = 49.25$ mm, $s_2 = 51.15$ mm

one were developed, namely: the mixed-mode I/II and II/III versions of the PENF, the mixed-mode I/III of the PSCB and the mixed-mode I/II PELS. The experiments were performed for the same E-glass/polyester material [24], [27], [30], [33]. The results of the IBT technique were compared to that of the compliance calibration (CC) method leading to a very good agreement between them [24], as a matter of fact the IBT was successfully applied for other tests. It is well-known that the CC method is reliable for the data reduction in common mode-I and mode-II tests. Furthermore, it may be assumed that the additional material properties were determined with an efficient accuracy for the former systems and they can be utilized also for the PSCB$_{II/III}$ system.

D. Fracture envelopes

Based on the nature of the reduced G_{II}-G_{III} data the so-called exponential hackle criterion was found to be reasonable to construct the fracture envelope in the G_{II}-G_{III} plane. The exponential hackle criterion is given by [38]:

$$G_{II} + G_{III} = (G_{IIIC} - G_{IIC})e^{\gamma(1-N)} \qquad (26)$$

where:

$$N = \sqrt{1 + \frac{G_{II}}{G_{III}}\sqrt{\frac{E_{11}}{E_{33}}}} \qquad (27)$$

which is an implicit mathematical function. In Eqs.(26)-(27) G_{IIC} is the critical ERR under pure mode-II (calculated from the data of the ELS specimen), G_{IIIC} is the mode-III critical ERR (calculated from the data of the MSCB specimen). The results of the PSCB$_{II/III}$ test listed in Table II (IBT) were
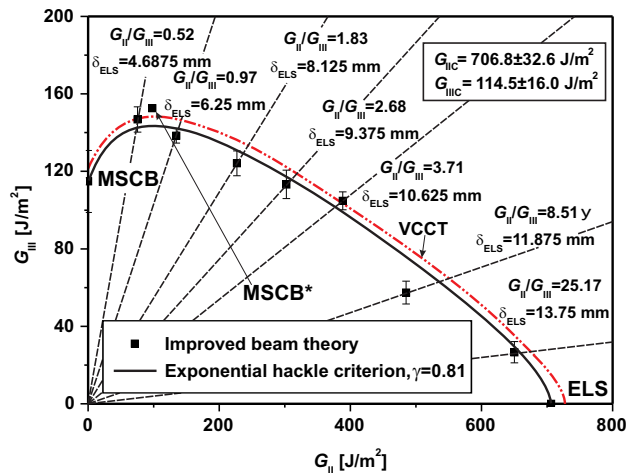

Fig. 10. Interlaminar fracture envelopes in the G_{II}-G_{III} plane for E-glass/polyester composite material determined by the IBT and VCCT methods.

used to provide seven additional points in the G_{II}-G_{III} plane. The power parameter in Eq.(26) and the fracture envelope was calculated in the code MAPLE [39]. The fracture envelope calculated by the IBT and VCCT methods is displayed in Fig.10. The shape of the curves is convex, in contrast with some previous results [30], [33]. The main conclusion is that there is a significant interaction between the mode-II and mode-III ERRs, especially if G_{II}/G_{III} is small. The scatter is also in reasonable ranges and it decreases with the increase of G_{IIC}. The red curve shows the result of the VCCT method, here we applied the widthwise average values of the ERRs. It is seen that the curve is similar to that obtained by IBT,

but IBT is more conservative. An additional point denoted by MSCB* can be found in Fig.10. This point was not considered when we calculated the envelope. The point was obtained by an MSCB measurement with s_1=25.69 mm, s_2=22.01 mm and a = 105 mm, i.e. under mixed-mode II/III condition without prestressing the specimen. The point represents again the average ERR obtained by VCCT calculation. We can see that this point absolutely fits into the curve. Therefore it may be assumed that the critical energy release rate is independent on the distribution of the ERR over the specimen width and the criterion of the average ERR is reasonable. However, to confirm this assumption more measurements are necessary.

In some recent works the fracture envelopes in the G_I-G_{II} and G_I-G_{III} planes were constructed by the mixed-mode I/II PELS and the mixed-mode I/III version of the PSCB specimen (PELS$_{I/II}$ and PSCB$_{I/III}$) for the same E-glass/polyester material [27], [33]. Similar experimental studies resulted in a concave envelope in the G_I-G_{II} and even a concave one in the G_{II}-G_{III} plane as it is shown in Figs.11a and b. It is important to note, that all of the envelopes in Figs.10 and 11a-b were determined for the same crack length (a=105 mm). Based on the comparison between Fig.10 and Figs.11a-b we may conclude that the material behaves differently under mixed-mode II/III than under mixed-mode I/II and I/III loading conditions, but proves similar behavior in the G_I-G_{II}, and the G_I-G_{III} planes. It is also important to note that interaction takes place in each case.

VIII. CONCLUSION

In this work the mixed-mode II/III version of the prestressed split-cantilever beam specimen was developed for interlaminar fracture testing of laminated transparent composite materials. Apart from the MSCB and the traditional ELS tests, the PSCB$_{II/III}$ specimen was used to obtain the mixed-mode II/III energy release rate at crack propagation onset including seven different mode ratios. To perform the experiments unidirectional E-glass/polyester specimens were manufactured. An improved beam model was recommended for the evaluation of both the mode-II and mode-III energy release rate. Finite element analysis was performed and it was shown that the mode ratio changes significantly along the specimen width and it is not possible to eliminate this variation.

The beam theory expressions give a widthwise average value of the energy release rates and mode ratio compared to the finite element results. Therefore the average energy release rate criterion was introduced and applied in the evaluation of the experimental data, namely the widthwise average values were believed to give acceptable and realistic results. The crack initiation was expected at the point where the maximum of the total energy release rate was calculated. Based on the performed experimental work the fracture envelope of the present material was determined indicating significant interaction between G_{II} and G_{III}.

One of the advantages of the PSCB$_{II/III}$ specimen is that it incorporates the traditional beam-like specimen geometry. Although the experiments were performed on unidirectional samples, it is possible to test specimens with other, symmetric
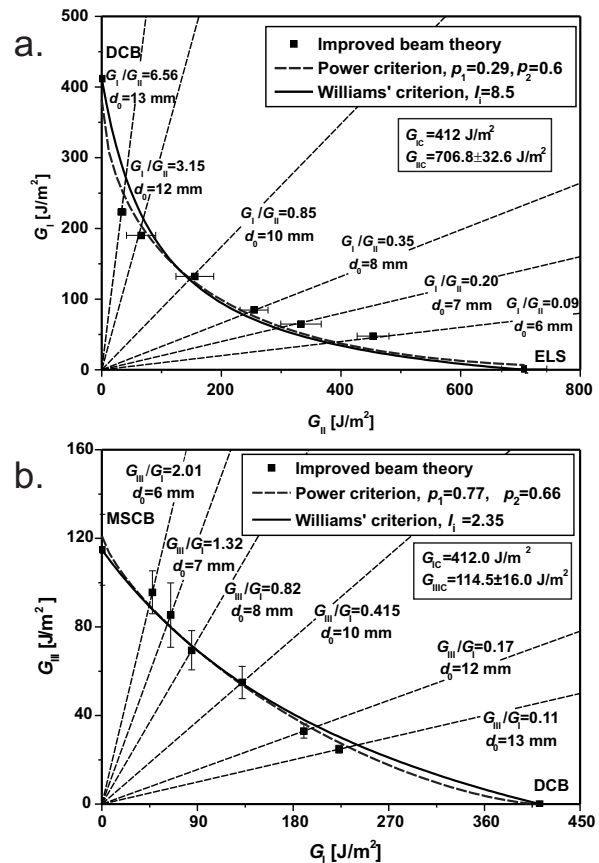

Fig. 11. Interlaminar fracture envelopes in the G_{II}-G_{III} plane for E-glass/polyester composite material determined by the IBT and VCCT methods.

lay-ups. Second, it was shown that the PSCB$_{II/III}$ specimen is able to produce any mode ratio at crack propagation onset. The drawbacks of the PSCB specimen are the low compliance values; the mode ratio changes with the crack length and the applied load, so the method is recommended mainly for the testing of transparent composite materials. Moreover the mode ratio changes significantly along the crack front. Finally, the mode ratio can not be calculated without performing experiments, i.e. it can not be designated before the test, involving the fact that the mode ratio will depend on the definition of the crack initiation and the accuracy of the measurement of the load and crack length. More research is needed to reduce the drawbacks of the test and to make it possible to test non-transparent materials

Szekrényes) for the construction of the experimental equipment.

REFERENCES

[1] T. L. Anderson, *Fracture Mechanics - Fundamentals and Applications*, third edition ed. Boca Raton, London, New York, Singapore: CRC Press, Taylor & Francis Group, 2005.

[2] A. J. Brunner and P. Flüeler, "Prospects in fracture mechanics of "engineering" laminates," *Engineering Fracture Mechanics*, vol. 72, pp. 899–908, 2005.

[3] A. J. Brunner, B. R. K. Blackman, and P. Davies, "A status report on delamination resistance testing of polymer-matrix," *Engineering Fracture Mechanics*, vol. 75, pp. 2779–2794, 2008.

[4] *ASTM D6671 / D6671M - 06 Standard Test Method for Mixed Mode I-Mode II Interlaminar Fracture Toughness of Unidirectional*, 2006.

[5] *Determination of the mixed-mode I/II delamination resistance of unidirectional fibre-reinforced polymer laminates using the asymmetric double cantilever beam specimen (ADCB)*, version 00-05-03 ed., European Structural Integrity Society (ESIS), Polymers and Composites Task Group, 2000.

[6] G. Becht and J. W. G. Jr., "Design and analysis of the crack rail shear specimen for mode III interlaminar fracture," *Composites Science and Technology*, vol. 31, pp. 143–157, 1988.

[7] S. L. Donaldson, "Mode III intelaminar fracture characterization of composite materials," *Composites Science and Technology*, vol. 32, pp. 225–249, 1988.

[8] S. M. Lee, "An edge crack torsion method for mode III delamination fracture testing," *Journal of Composite Technology & Research*, vol. 15, no. 3, pp. 193–201, 1993.

[9] W. C. Liao and C. T. Sun, "The determination of mode III fracture toughness in thick composite laminates," *Composites Science and Technology*, vol. 56, pp. 489–499, 1996.

[10] H. Suemasu, "An experimental method to measure the mode-III interlaminar fracture toughness of composite materials," *Composites Science and Technology*, vol. 59, pp. 1015–1021, 1999.

[11] J. G. Ratcliffe, "Characterization of the edge crack torsion (ECT) test for mode III fracture toughness measurement of laminated composites," NASA, Technical Memorandum 213269, 2004.

[12] D. Pennas, W. J. Cantwell, and P. Compston, "The influence of strain rate on the mode III interlaminar fracture of composite materials," *Journal of Composite Materials*, vol. 41, pp. 2395–2614, 2007.

[13] A. B. de Morais, A. B. Pereira, M. F. S. F. de Moura, and A. G. Magalhães, "Mode III interlaminar fracture of carbon/epoxy laminates using the edge crack torsion (ECT) test," *Composites Science and Technology*, vol. 69, pp. 670–676, 2009.

[14] P. Robinson and Q. D. Song, "The development of an improved mode III delamination test for composites," *Composites Science and Technology*, vol. 52, pp. 217–233, 1994.

[15] D. Cicci, F. Sharif, and M. T. Kortschot, "Data reduction for the split cantilever beam mode III delamination test," in *Proceedings, ACCM 10*, Whistler, British Columbia, Canada, 14-18 August 1995, pp. 1–8.

[16] F. Sharif, M. T. Kortschot, and R. H. Martin, "Mode III delamination using a split cantilever beam," in *Composite Materials: Fatigue and Fracture - Fifth Volume*, R. H. Martin, Ed., vol. ASTM STP 1230. Philadelphia: ASTM, 1995, pp. 85–99.

[17] K. Trakas and M. T. Kortschot, "The relationship between critical strain energy release rate and fracture mode in multidirectional carbon-fiber/epoxy laminates," in *Composite Materials: Fatigue and Fracture - Sixth Volume*, A. Armanios, Ed., vol. ASTM STP 1285. ASTM, 1997, pp. 283–304.

[18] V. Rizov, Y. Shindo, K. H. K, and F. Narita, "Mode III interlaminar fracture behaviour of glass fiber reinforced polymer woven laminates at 293 to 4 k," *Applied Composite Materials*, vol. 13, pp. 287–304, 2006.

[19] M. Farshad and P. Flüeler , "Investigation of mode III fracture toughness using an anti-clastic plate bending method," *Engineering Fracture Mechanics*, vol. 60, pp. 5–6, 1998.

[20] H. Yoshihara, "Examination of the 4-ENF test for measuring the mode III R-curve of wood," *Engineering Fracture Mechanics*, vol. 73, pp. 42–63, 2006.

[21] A. B. de Morais and A. B. Pereira, "Mode III interlaminar fracture of carbon/epoxy laminates using a four-point bending plate test," *Composites Part A - Applied Science and Manufacturing*, vol. 40, no. 11, pp. 1741–1746, 2009.

[22] A. Szekrényes, "Improved analysis of the modified split-cantilever beam for mode-III fracture," *International Journal of Mechanical Sciences*, vol. 51, pp. 682–693, 2009.

[23] A. B. Pereira, A. B. de Morais, and M. F. S. F. de Moura, "Design and analysis of a new six-point edge crack torsion (6ECT) specimen for mode III interlaminar fracture characterisation," *Composites Part A - Applied Science and Manufacturing*, vol. 42, no. 2, pp. 131–139, 2011.

[24] A. Szekrényes, "Delamination fracture analysis in the G_{II}-G_{III} plane using prestressed transparent composite beams," *International Journal of Solids and Structures*, vol. 44, pp. 3359–3378, 2007.

[25] A. B. Pereira and A. B. de Morais, "Mixed mode I+III interlaminar fracture of carbon/epoxy laminates," *Composites Part A - Applied Science and Manufacturing*, vol. 40, no. 4, pp. 518–523, 2009.

[26] A. B. de Morais and A. B. Pereira, "Mixed mode II+III interlaminar fracture of carbon/epoxy laminates," *Composites Part A - Applied Science and Manufacturing*, vol. 68, no. 9, pp. 2022–2027, 2008.

[27] A. Szekrényes, "Interlaminar fracture analysis in the G_I-G_{III} plane using prestressed transparent composite beams," *Composites Part A - Applied Science and Manufacturing*, vol. 40, no. 10, pp. 1621–1631, 2009.

[28] H. Suemasu, A. Kondo, K. Gozu, and Y. Aoki, "Novel test method for mixed mode II and III interlaminar fracture toughness," *Advanced Composite Materials*, vol. 19, pp. 349–361, 2010.

[29] R. M. Marat-Mendes and M. M. Freitas, "Failure criteria for mixed mode delamination in glass fibre epoxy composites," *Composite Structures*, vol. 92, no. 9, pp. 2292–2298, 2010, fifteenth International Conference on Composite Structures.

[30] A. Szekrényes, "Prestressed fracture specimen for delamination testing of composites," *International Journal of Fracture*, vol. 139, pp. 213–237, 2006.

[31] M. Kenane and S. Benmedakhene, "Fracture and fatigue study of unidirectional glass/epoxy laminate under different mode of loading," *Fatigue and Fracture of Engineering Materials & Structures*, vol. 33, no. 5, pp. 284–293, 2010.

[32] A. Szekrényes, "Improved analysis of unidirectional composite delamination specimens," *Mechanics of Materials*, vol. 39, pp. 953–974, 2007.

[33] A. Szekrényes, "Prestressed composite specimen for mixed-mode I/II cracking in laminated materials," *Journal of Reinforced Plastics and Composites*, vol. 29, pp. 3309–3321, 2010.

[34] N. K. Naik, K. S. Reddy, S. Meduri, N. B. Raju, P. D. Prasad, S. N. M. Azad, P. A. Ogde, and B. C. K. Reddy, "Interlaminar fracture characterization for plain weave fabric composites," *Journal of Materials Science*, vol. 37, pp. 2983–2987, 2002.

[35] S. F. Hwang and C. L. Hu, "Tearing mode interlaminar fracture toughness of composite materials," *Polymer Composites*, vol. 22, pp. 57–64, 2001.

[36] N. Blanco, E. K. Gamstedt, J. Costa, and D. Trias, "Analysis of the mixed-mode end load split delamination test," *Composite Structures*, vol. 76, pp. 14–20, 2006.

[37] H. Yoshihara and A. Satoh, "Shear and crack tip deformation correction for the double cantilever beam and three-point end-notched flexure specimens for mode i and mode ii fracture toughness measurement of wood," *Engineering Fracture Mechanics*, vol. 76, pp. 335–346, 2009.

[38] J. R. Reeder, "An evaluation of mixed-mode delamination failure criteria," NASA, Technical Memorandum 104210, 1992.

[39] F. Garvan, *The Maple Book*. Boca Raton, London, New York, Washington D.C.: Chapman & Hall/CRC, 2002.